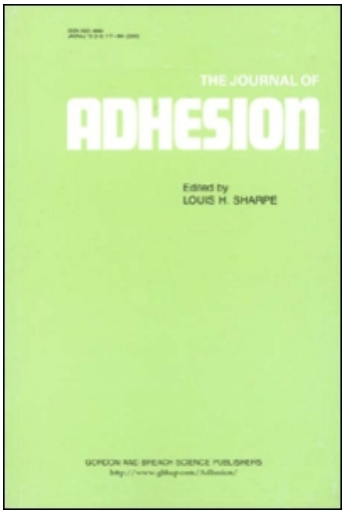

The Journal of Adhesion
Publication details, including instructions for authors and subscription information:
http://www.informaworld.com/smpp/title~content=t713453635

Evaluation of Adhesion Property of UHMWPE Fibers/Nano-epoxy by a Pullout Test

Soumen Jana[a]; Aruna Zhamu[a]; Wei-Hong Zhong[a]; Yong Xue Gan[b]
[a] Department of Mechanical Engineering and Applied Mechanics, North Dakota State University, Fargo, North Dakota, USA [b] Department of Mechanical Engineering, Albert Nerken School of Engineering, Cooper Union for the Advancement of Science and Art, New York City, New York, USA

To cite this Article Jana, Soumen , Zhamu, Aruna , Zhong, Wei-Hong and Gan, Yong Xue(2006) 'Evaluation of Adhesion Property of UHMWPE Fibers/Nano-epoxy by a Pullout Test', The Journal of Adhesion, 82: 12, 1157 — 1175
To link to this Article: DOI: 10.1080/00218460600998763
URL: http://dx.doi.org/10.1080/00218460600998763

The Journal of Adhesion, 82:1157–1175, 2006

ISSN: 0021-8464 print/1545-5823 online
DOI: 10.1080/00218460600998763

Taylor & Francis
Taylor & Francis Group

Evaluation of Adhesion Property of UHMWPE Fibers/ Nano-epoxy by a Pullout Test

Soumen Jana
Aruna Zhamu
Wei-Hong Zhong
Department of Mechanical Engineering and Applied Mechanics, North Dakota State University, Fargo, North Dakota, USA

Yong Xue Gan
Department of Mechanical Engineering, Albert Nerken School of Engineering, Cooper Union for the Advancement of Science and Art, New York City, New York, USA

Ultrahigh-molecular-weight polyethylene (UHMWPE) fibers have poor wetting and adhesion properties to polymer resins because of the inert surface of the fibers. In our previous study, a reactive nano-epoxy matrix, developed by making a modification on the matrix with reactive graphitic nanofibers (r-GNFs), showed improved wettability to UHMWPE fibers. In this work, fiber bundle pullout tests were conducted to evaluate the adhesion property between the UHMWPE fibers and the nano-epoxy matrices. Analysis of load–displacement curves from pullout tests shows that debonding initiation load and ultimate debonding load increased considerably, because of effective improvement of adhesion between the UHMWPE fibers and nano-epoxy matrix. Stress-controlled and energy-controlled models of interfacial debonding were applied for theoretical analyses. Results from ultimate IFSS, frictional shear stress, and critical energy-release rate are in good agreement with experimental results. Nano-epoxy matrix with 0.3 wt% r-GNFs shows effective improvement in terms of adhesion property between UHMWPE fiber and epoxy.

Keywords: Epoxy; Graphitic nanofibers; Interfacial adhesion; Pullout test; Ultrahigh molecular polyethylene (UHMWPE) fiber

Received 11 March 2006; in final form 3 Augutst 2006.
Address correspondence to W. H. Zhoung, Department of Mechanical Engineering and Applied Mechanics, North Dakota State University, Fargo, ND 58105, USA. E-mail: Katie.zhong@ndsu.edu

1. INTRODUCTION

Ultrahigh-molecular-weight polyethylene (UHMWPE) fibers have good mechanical and physical properties. The fibers are also effective as shielding materials against galactic cosmic rays because of the presence of a high amount of hydrogen in the UHMWPE; thus, they are suitable for applications in space missions [1]. However, UHMWPE fibers have poor wettability and adhesion to polymer resins [2,3]. Though some surface treatments can be used to improve the interfacial adhesion between the fibers and polymer matrices [2–9], we are more interested in improving the interfacial properties by modifying the matrices using functionalized nanoscale additives. Graphitic nanofibers (GNFs) are readily available in large volume at relatively low cost [10–13]. The edges of graphene planes in the GNFs may be utilized to attain chemical functionalization of the GNFs and serve as reaction agents with bifunctional linkers, which can promote covalent bonding between the GNFs and the polymer resin molecules [14,15]. Some research results of reinforced composites using nanofillers and epoxy resins have been reported [16–25]. However, there are very few research papers on improving mechanical properties of UHMWPE/polymer matrix composites using a small amount of the nanofillers (less than 1 wt%).

In our previous research, functionalized herringbone graphitic nanofibers with 3,4′ -oxydianiline (GNF-ODA) (Figure 1) were fabricated into r-GNFs (Figure 2) [15,26,27]. The reactive hydrogen in the −OH− group of the r-GNFs could be involved in the curing reaction among epoxy resins as an amine-type curing agent does and allow the r-GNFs to be incorporated into the cured epoxy matrix structures. Therefore, this r-GNF/epoxy, as a unified resin system, became a real matrix, instead of a mixture or a simple nanocomposite [26,27]. Our previous work on the nano-epoxy matrix materials with lower concentration of r-GNFs (less than 1 wt %) showed enhanced mechanical properties in UHMWPE/nano-epoxy composites and improved wettability to the UHMWPE fibers [28].

Various test methods such as pullout, push-out, microbond, and fragmentations have been extensively used to evaluate the efficiency

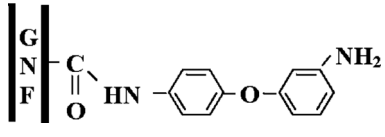

FIGURE 1 Structure of GNF-ODA nanofiber.

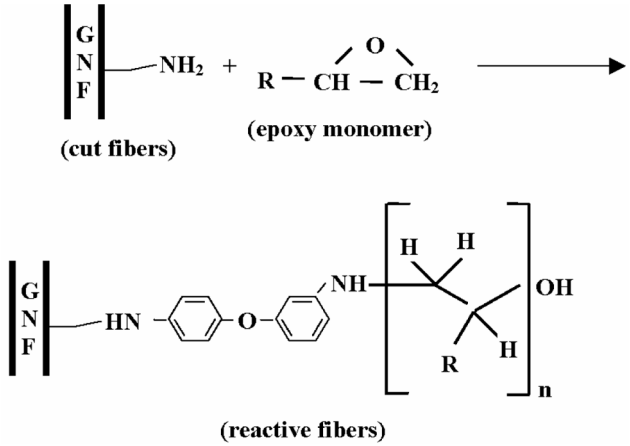

FIGURE 2 Formation of an r-GNF [26,27].

of load transfer between a fiber and a matrix through the interface. In this work, a fiber bundle pullout test was applied to evaluate the adhesion property in UHMWPE fibers/nano-epoxy. Load-displacement curves from pullout tests were analyzed. Results showed effective improvement in the fiber/nano-matrix interfacial property. Study results from stress- and energy-based models of interfacial debonding showed that they were in good agreement with experimental results.

2. EXPERIMENTS

UHMWPE fibers (Spectra® 1000) were purchased from Honeywell Co., Colonial Heights, VA, USA Epoxy resins (Epon® 828 Resin and Epon® 815 C), Versamid 140 (curing agent), cure agents (Epikure(tm) W, diethyltoluenediamine, and Versamid 140), and accelerator (Epikure(tm) 537) were purchased from Miller-Stephenson Chemical Inc., Danbumg, CT, USA. Functionalized graphitic nanofibers, GNF-ODA (Figure 1), were provided by Vanderbilt University, Nashville, TN, USA. A reactive diluent from Sigma-Aldrich Co., Milwaukee, WI, USA, butyl glycidyl ether (BGE), has an epoxy group similar to that found in epoxy resins, but the viscosity of the diluent is much lower compared with the epoxy resins.

A mixture of GNF-ODA nanofibers and diluent (BGE) (1:50 by weight) was mixed by sonication (Branson® 450, Damburg, CT, USA)

at a power level 70 w for 3 h at room temperature. Such a sonication treatment can reduce the length of the GNF-ODA nanofibers to 400–800 nm but it does not change the diameter of the nanofibers ($25 \sim 100$ nm). These small GNF-ODA nanofibers were allowed to react with BGE for 36 h, and thus, r-GNFs were obtained as shown in Figure 2 [26,27]. The solution was vacuumed in a hot vacuum chamber to control the r-GNF/BGE ratio to 1:6 by weight.

The curing agent was added to the 828 epoxy in a ratio of 24:100 by weight. The accelerator was added to the epoxy matrix in 1:200 by weight to lower the curing temperature of the matrix and prevent the UHMWPE fibers from melting. The pure epoxy matrix contains the curing agent and the accelerator. Proper amounts of r-GNF/dilu-diluent solutions were added to the pure epoxy matrix to make nano-epoxy matrices having 0.1, 0.2, 0.3, 0.5 and 0.8% r-GNFs loadings by weight. Low-level sonication was conducted for each mixture for an hour at room temperature to disperse the r-GNFs into the pure epoxy matrix.

The UHMWPE fiber bundles were coated with different matrix solutions using a soft brush, which resulted in a layer of matrix over fiber bundles. The matrix-coated bundles were cured for 4 h at 120°C and then cooled naturally to room temperature. The ends of the specimens for clamping during pullout tests were prepared through the following steps: the coated bundles were put into cylindrical molds, another type of epoxy matrix (in this article termed the clamping matrix: a mixture of Epon 815 C and Versamid 140 at ratio of 100:20) was poured into the molds; cured for 3 h at a temperature of 100°C, and then cooled down naturally to room temperature (Figure 3(a,b). The embedded length (H) of specimens was fixed by removing the extra length of the clamping matrix through grinding. The free length, a, for all the specimens was 5 mm and was controlled strictly, because the length would affect the pull-out curves. Pullout tests were conducted on a Q-test machine from MTS Systems Corporation, Cary, NC, USA, at room temperature. The crosshead speed was 1.0 mm/min. Three sets of embedded lengths (17 mm, 20 mm, and 23 mm) were considered. There were six types (0, 0.1, 0.2, 0.3, 0.5, and 0.8 wt%) of specimens depending on the r-GNF content in the set of specimens with an embedded length of 17 mm. For the specimens with 20 mm and 23 mm embedded lengths, we used two types of matrices: pure epoxy and nano-epoxy with 0.3 wt % of r-GNFs. Ten specimens from each type in each group were tested. Load *vs.* displacement curves from such pullout tests on each specimen were recorded for analysis.

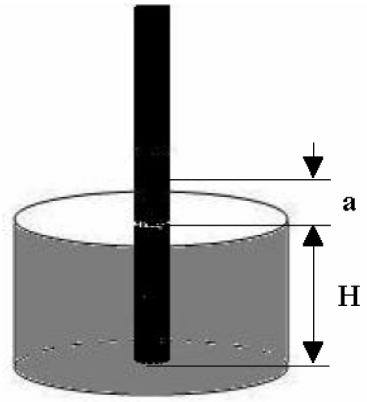

(a)

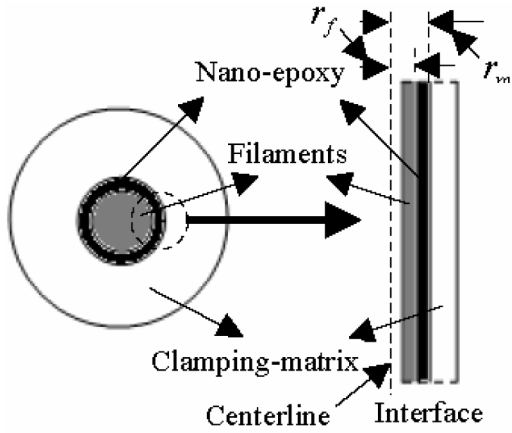

(b)

FIGURE 3 (a) Schematic design of specimen for pullout test; (b) Schematic design of interface between bundle and matrix.

3. RESULTS AND DISCUSSION

3.1. Load-Displacement Behavior

A typical load *vs.* displacement curve obtained from the pullout tests is shown in Figure 4a. Figure 4b and c show the details in two different parts with distinct characteristics. The load *vs.* displacement curves of the UHMWPE fiber/matrix specimens with different r-GNF contents gave a very similar shape. From Figure 4a–c, it can be seen that the curves show four segments: 1) segment *A*: elastic behavior of the part

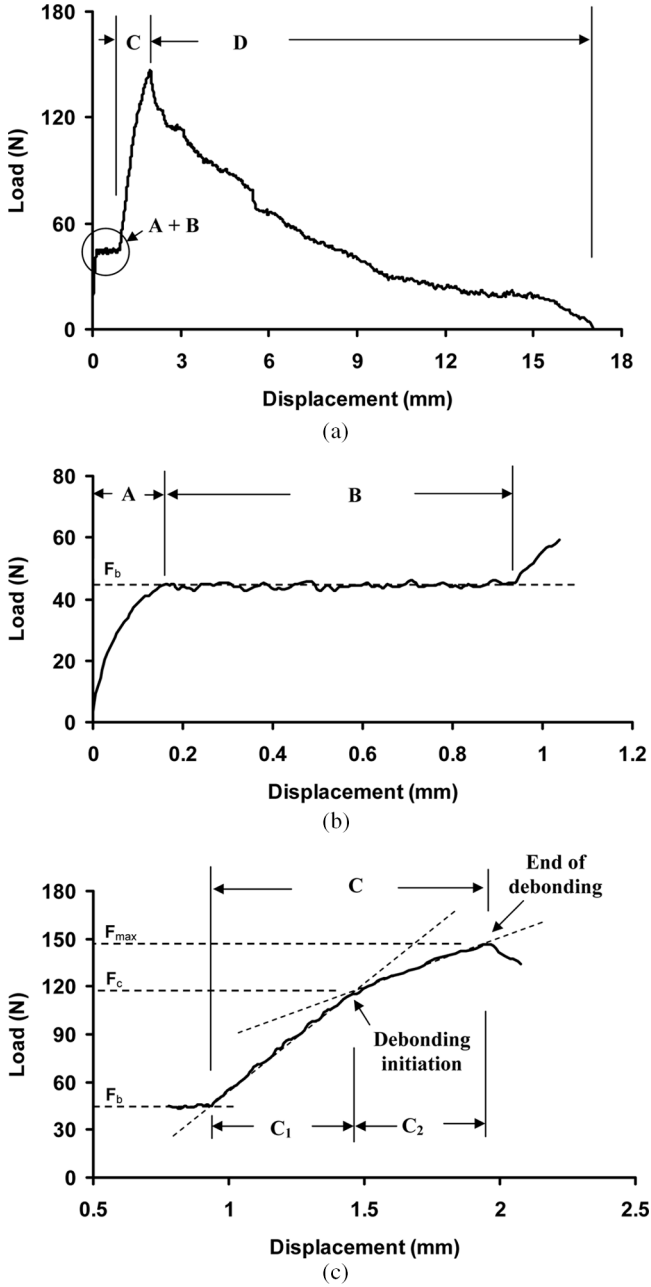

FIGURE 4 Typical curve of load *vs*. displacement under pullout test: (a) complete curve; (b) portions of *A* and *B*; and (c) portion of *C*.

with a free-length, a (Figure 3a); 2) segment B: onset of matrix cracking, crack multiplication and debonding between the UHMWPE fibers and the matrix in free-length part a; 3) segment C: elongation of the UHMWPE fiber bundle at free-length a (subsegment C_1) and debonding of the UHMWPE fibers from the matrix at the embedded part H (subsegment C_2); and 4) segment D: pullout of the UHMWPE fibers from the debonded matrix in the embedded part, H (see Figure 3a).

During the initial stage of the pullout test, the nonembedded part (with a free length a) of the UHMWPE fiber/matrix specimen deforms elastically; the fiber reinforcement and the matrix stay as a unit without damage. This deformation stage portrays the segment A on the load–displacement curve as shown in Figure 4 a and b. Next to segment A, the nonembedded part of the specimen could no longer bear the progressively increasing strain and remain as a single unit, and, thus, onset of matrix cracking, crack multiplication, and debonding between the fibers and the matrix were the main phenomena, which is revealed by segment B on the load–displacement curve. The profile of the load–displacement curve found in our previous tensile tests on UHMWPE fiber/matrix bundle composites [29] was similar to what we observed in this pullout behavior of the free-length part of the specimen. For the free length a, with the increase of quasi-static load, the initial damage occurred through matrix cracking, the propagation direction of which is perpendicular to the long axis of the UHMWPE fibers. The first crack in the matrix was observed to propagate over the whole cross-sectional area of the matrix but was stopped by the UHMWPE fibers, and, thus, bundle failure did not occur immediately. At some small distance from the crack plane, the load was transferred back from UHMWPE fibers to the matrix and resulted in further cracking of the matrix. Crack density continuously increased with increase of the strain and created a plateau stage as shown in Figure 4b. The load required at this stage is $F_b$as marked on the curve.

In segment C (Figure 4a), a portion of a load-displacement curve, as shown in further detail in Figure 4c, reveals two characteristic events. The first event is the elastic elongation of the UHMWPE fiber bundle in the free-length region of the specimen, which was depicted on the load–displacement curve and demarcated as C_1. The second one is the debonding between the UHMWPE fibers and the matrix in the embedded part of the specimen, which was marked as C_2. The load–displacement curve in part C_1 is almost linear because it was due to the elongation of the UHMWPE fiber bundle elastically under the load between F_b and F_c (load corresponds to the debonding initiation). Although the elongation of the UHMWPE fiber bundle occurred in free-length ends, the UHMWPE fiber/matrix interface in the

embedded region remained intact. The displacement in the embedded region of a pullout specimen could be neglected before the debonding of the UHMWPE fibers from the matrix. Therefore, the load–displacement curve from the very beginning to the end of C_1 reveals the deformation behavior of the free–length part of a pullout specimen under the increasing load. The UHMWPE fibers started to debond from the matrix when the load reached a critical valueF_c, which is defined as the debonding initiation load. With the increase of the debonding force in stage C_2 ($F_c \leq F \leq F_{\max}$), interfacial cracks propagated along the interface of the fibers and the matrix; the frictional force from the debonded part of the embedded length was added to the adhesion force of the nonembedded portion. This debonding force depends upon the elastic constants of the materials, the initial crack size, the specimen dimensions, and the interfacial fracture energy [30–33]. At this stage, with the steady increase of the debonded fiber bundle, the embedded part was elongated with the increase in strain. Both these two occurrences at the same time made the slope of the load–displacement curve decrease gradually, starting from the debonding initiation point of stage C. There are at least two types of interfaces in each specimen: 1) the interface between the UHMWPE fibers and the matrix and 2) the interface between the matrix encapsulating the UHMWPE fibers and the clamping matrix. In addition, another interface between r-GNFs and matrix might also be activated in the pullout test. However, we observed only interfacial debonding between the UHMWPE fibers and the matrix, as there was no detectable resin left on the surface of UHMWPE filament surface (Figure 5). This phenomenon affirmed that the bundle pullout method used for characterization of interfacial adhesion between UHMWPE fibers and nanoepoxy in our experiment is effective.

When the debonding force reached $F_{\max}$, crack propagation became unstable, with a wholly debonded interface along the embedded length and the load dropped from the peak value. Segment D shown in Figure 4a represents the pullout of the UHMWPE fibers in the embedded region of the specimen from the matrix. The debonding caused the separation of the UHMWPE fibers from the matrix. After reaching the peak load $F_{\max}$, at the terminnation of stage C, the load decreased rapidly. After that, a reduced rate of decreasing load was observed. At this moment, the UHMWPE fiber bundle over all its length was pulled out. As the length of the bundle being pulled out was decreasing, the load required was going down with the increase in the crosshead displacement, as shown in Figure 4a. Elastic contraction of the UHMWPE fibers might happen following the debonding, depending on the interfacial parameters such as the interfacial frictional shear stress τ_f [34],

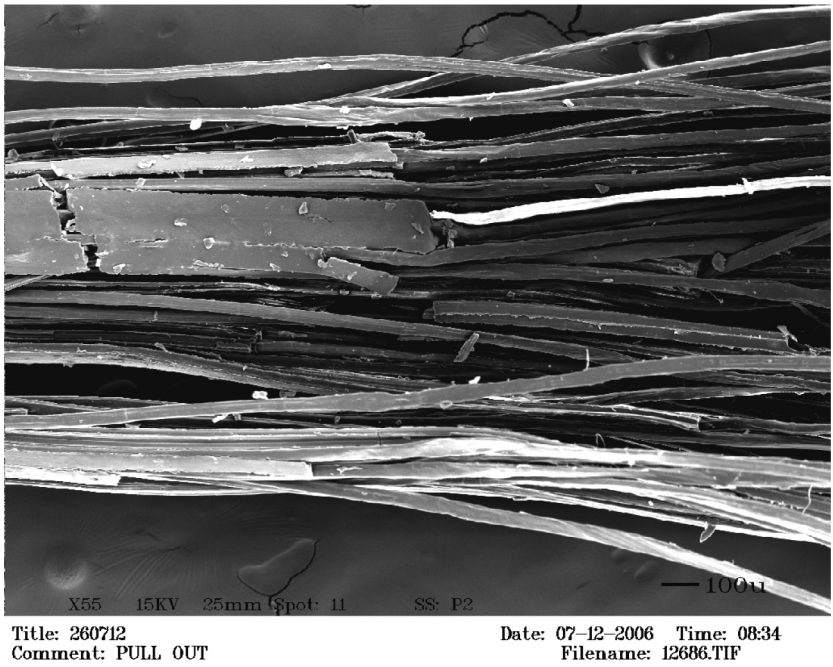

FIGURE 5 SEM image of tested bundle (from middle toward the left is the free-length part and toward the right is the embedded part).

the Coulomb friction coefficient μ_f [35], and the clamping stress q_c [35]. The interfacial friction coefficient between the matrix and the UHMWPE fibers was the key parameter to determine the load needed to pull the UHMWPE fibers out after their debonding from the matrix. If the interface between the fiber and the matrix is very strong, after debonding immediate extraction of the bundle might take place [36]. In the case of weak interfaces, the bundle might be extracted progressively [37], depending on those parameters mentioned before.

3.2. Effect of the r-GNFs

3.2.1. Experimental Analysis

Figure 6 represents the load–displacement curves of specimens with pure epoxy matrix and nano-epoxy matrix with 0.3 wt% of r-GNF. The shape of the curves for both type of specimens are similar. From this figure, it is easily observed that maximum debonding load ($F_{\max}$) in the nano-epoxy specimen is higher than that of the pure

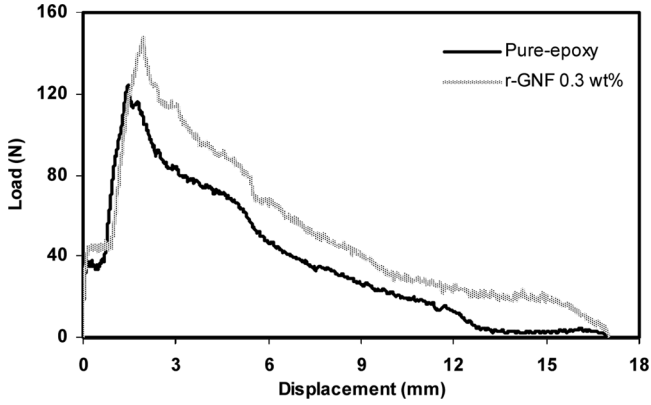

FIGURE 6 Load–displacement curves found in pullout tests of pure-epoxy and nano-epoxy (0.3 wt% r-GNF) specimens.

epoxy specimen. Besides, the debonding initiation load (F_c) is higher in the nano-epoxy specimen (not distinct in the figure). Figure 7 shows the maximum debonding loads, $F_{\max}$, and the debonding initiation loads obtained from the pullout tests on specimens with different r-GNF loading for the 17-mm embedded length. Among all types of the specimens with the 17-mm embedded length, the one containing 0.3 wt% r-GNF-shows the highest maximum debonding load, which is in agreement with our previous studies on microbond tests, and it is increased by 19% (from 122 ± 7.17 to 146 ± 5.67) over the pure

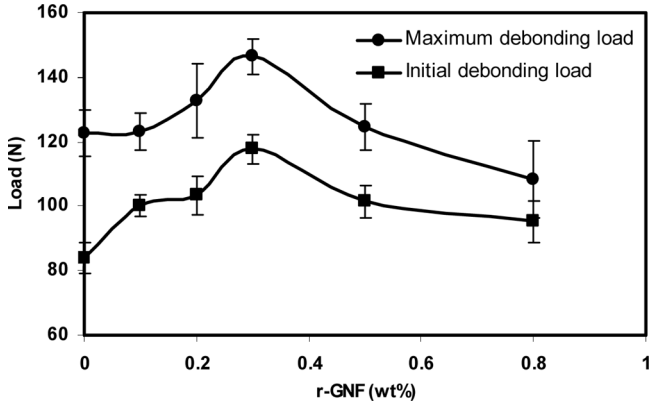

FIGURE 7 Initial debonding and maximum debonding load *vs*. r-GNF loading.

epoxy specimen. To confirm the effectiveness of nano-epoxy with 0.3 wt % of r-GNF over the pure epoxy, the pure epoxy and the 0.3-wt% r-GNF-loaded nano-epoxy specimens with 20-mm and 23-mm embedded lengths were prepared and tested. However, it was found that the UHMWPE fibers could not be pulled out effectively from the nano-epoxy specimens with the 23-mm embedded length. Therefore, no testing curves were recorded. For the specimen with the 20-mm embedded lengths, most of the UHMWPE fibers were pulled out from the nano-epoxy, which resulted in larger data deviation than the results from specimens of 17-mm embedded length. However, the UHMWPE fibers were completely pulled out from all the pure-epoxy specimens. Such experimental results indicate that the nano-epoxy is effective in enhancing interfacial properties to the UHMWPE fibers. Figure 8 depicts the maximum debonding load for the specimens with 17-mm and 20-mm embedded lengths, each containing pure epoxy and 0.3 wt% r-GNF-loaded matrices, which show higher maximum debonding loads in the nano-epoxy specimens over pure epoxy specimens. Differences in the peak loads between the specimens with 17-mm and 20-mm embedded lengths with or without 0.3-wt% r-GNFs are very small. It is expected that if all UHMWPE fibers could be pulled out from the nano-epoxy material for 20-mm embedded length specimens, the peak load values would be higher than the values shown in Figure 8. The most effective value of debonding initiation load was found in specimens with 0.3-wt% r-GNF loading

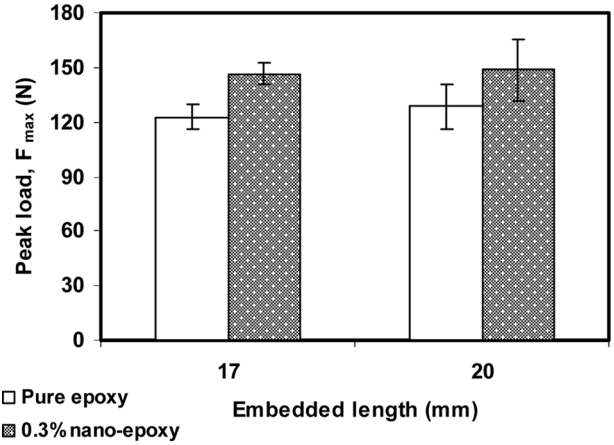

FIGURE 8 Maximum debonding load, F_{max}, for the pullout specimens with 17 mm and 20 mm embedded.

compared with pure epoxy and other nano-epoxy matrix specimens, and the increment was $\sim$39% (from 84 ± 4.65 to 117 ± 4.34 N). However, higher concentration of r-GNF in the matrix does not show better interfacial properties (Figure 7).

During curing, epoxy molecules formed a three-dimensional (3-D) cross-link network. Covalent bonding was also generated between the r-GNFs and the epoxy resin molecules in the nano-epoxy specimens. As a result, in nano-epoxy specimens, both 3-D networks and covalent bonds were present, and the covalent bonding strengthened the 3-D networks of the epoxy molecules. In brief, the characteristic loads demonstrate that the nano-epoxy matrix can improve the interfacial property of the UHMWPE fibers to the epoxy matrix. Moreover, the optimum amount of nanofiber addition to the specimens is 0.3 wt%.

To explain the mechanisms of the improvement in the interfacial adhesion between the UHMWPE fibers and the matrix, a model shown in Figure 9 was proposed. Our previous work shows that the nano-epoxy improved the wettability of UHMWPE fibers [28]. Therefore, before the curing of the matrix, the nano-epoxy wets the UHMWPE fiber surface because of the existence of the active r-GNF in the matrix. The activities of the r-GNF are determined by two factors. One is the cutting procedure, which resulted in the fresh ends on the nanofibers because the functionalized GNF-ODA nanofibers were cut first in the presence of the reactive diluent, BGE, which also served as a dispersant. This cutting process resulted in fresh and active ends of the nanofibers, and the fresh ends were protected by the BGE diluent, which makes the r-GNF physically absorbed onto UHMWPE fiber surface. More important are the highly polarized and reactive nanofibers, r-GNFs, formed through the reaction between

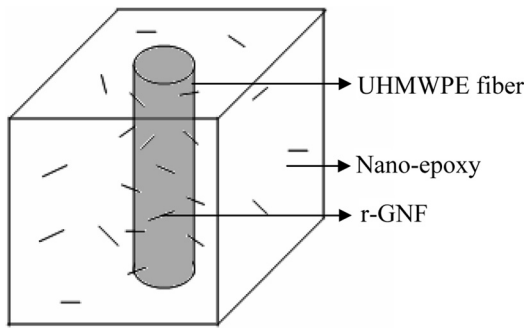

FIGURE 9 Sketch of r-GNFs on UHMWPE fibers.

the linker (ODA) and the oxirane group in the reactive diluent BGE [15,26,27]. Therefore, during the nano-epoxy wetting process, many of the r-GNFs attached onto the UHMWPE fiber surface. Following the curing procedures for the UHMWPE fibers/nano-epoxy, the nanofibers were fixed to the UHMWPE fiber surface. The r-GNFs also resulted in enhanced mechanical properties for the nano-epoxy matrix [38]. Therefore, the structure shown in Figure 9 formed. It is the r-GNFs on the UHMWPE fiber surface that help resist the UHMWPE fibers being pulled out from the matrix materials, resulting in higher forces and energy for completing the pullout processes. More studies regarding this proposed model shown in Figure 9, are being conducted through nanoindentation.

The interfacial property of the specimens with a higher amount of nanofibers such as 0.5 and 0.8 wt% of r-GNFs degraded slightly as compared with that of the specimens with 0.3 wt% of r-GNFs. This phenomenon may be due to the effect of a higher amount of the diluent's molecules remaining in the matrix. Because the r-GNFs are highly polarized and reactive, the use of the diluent, initially as a dispersant for the cutting process, is necessary to prevent the agglomeration of r-GNFs. In this study, the saturated solution of r-GNFs in the diluent has a fixed ratio, 1:6, of the r-GNFs to the diluent by weight. For the specimens with 0.1, 0.2, and 0.3 wt% of r-GNF, the contents of the diluent used in the specimens are relatively small: 0.6 wt% ($=0.1\times6$), 1.2 wt% ($=0.2\times6$), and 1.8 wt% ($=0.3\times6$), respectively. When the content of the diluent is increased further (higher r-GNF wt%), the percentage of r-GNFs on the UHMWPE fiber surface during the wetting process is decreased in the overall matrix system, and consequently, the contribution of r-GNFs to adhesion property is decreased because of the obvious diluent effect.

These results imply that there is an optimal concentration of r-GNFs, which is about 0.3 wt%. At this level, the most effective improvement of the interfacial properties between the UHMWPE fiber and the matrix is achieved.

3.2.2. Theoretical Analysis Using Fracture Mechanics

Several models describing stress distribution and interfacial failure in fiber-matrix system have been proposed by different researchers. These models can be divided into two categories. One is stress-controlled debonding and other is energy-controlled debonding. In our experiment, the bundle is coated with matrix, and therefore, the fiber bundle can be assumed to be a single fiber for the sake of theoretical analysis. Though frictional force and other parameters might come into play among filaments of the bundle, they can be ignored

in getting relative performance, as they affect the results in a similar way for each type of specimen.

In stress-controlled debonding, the ultimate interfacial frictional shear stress (IFSS), τ_{ult}, which is the local shear stress required to produce debonding near the crack tip, is an interfacial parameter [39]. One-dimensional shear-lag analysis can be used to calculate ultimate interfacial shear strength by the following equation [40]:

$$\tau_{ult} = \frac{F_c \beta}{2\pi r_f \tanh(\beta l_e)} + \tau_{therm} \cdot \tanh\left(\frac{\beta l_e}{2}\right). \quad (1)$$

Equation (1) shows that τ_{ult} depends on debonding load and thermal stress, τ_{therm}, which evolves because of the difference in coefficient of thermal expansion (CTE) of fiber and matrix. τ_{ult} has been calculated considering the debonding initiation load (F_c). Variables r_f and r_m are the radii of fiber bundle and matrix, respectively; E_f is the tensile modulus of the fiber; α_f and α_m are the coefficients of thermal expansion of fiber and matrix, respectively; ΔT is the difference between test temperature and stress-free temperature; l_e is the embedded length; and β is the shear-lag parameter, which can estimated using Cox's shear-lag analysis by the following equation [41]:

$$\beta = \left(\frac{2G_m}{E_f r_f^2 \ln(r_m/r_f)}\right)^{1/2}. \quad (2)$$

Thermal stress can be evaluated using the following equation [39]:

$$\tau_{therm} = E_f \beta r_f (\alpha_f - \alpha_m)\left(\frac{\Delta T}{2}\right). \quad (3)$$

The friction force between the UHMWPE fiber and the matrix at the debonded region can be used to accurately characterize the adhesion property. IFSS, τ_f (another interfacial parameter), due to friction in the debonded region, has been assumed to be constant. Equation (4) can be used to determine IFSS for different matrix systems:

$$\tau_f = \frac{F_{\max}}{2\pi r_f l_e}. \quad (4)$$

Values of τ_f for different matrix systems were measured using the maximum debonding load. Figure 10 shows ultimate IFSS, frictional shear stress, and thermal stress *vs*. r-GNF concentration using property values of the different materials listed in Table 1. Both ultimate

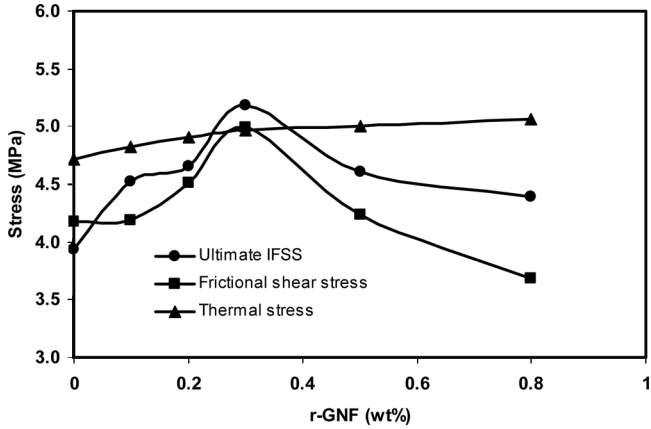

FIGURE 10 Ultimate IFSS, frictional shear stress, and thermal stress *vs.* r-GNF loading.

IFSS and frictional shear stress were the highest for the specimen with 0.3 wt% of r-GNF. Ultimate IFSS in the 0.3 wt% r-GNF specimen was increased by $\sim$32% (from 3.93 to 5.18 MPa) over pure epoxy, and for frictional shear stress, the increment was $\sim$19% (from 4.18 to 4.99 MPa) over pure epoxy. Thermal stress increased with increase in r-GNF concentration, as the difference between CTE of fiber and CTE of matrices were increasing with increased r-GNF content.

In energy-controlled debonding, the energy release rate, G, which is the amount of energy released per unit of debonded area in the specimen, is a possible criterion for comparing interfacial properties. If G reaches the critical value G_{ic} for crack initiation/extension, the debonding zone will extend. The critical energy release rate, G_{ic}, can be estimated by the following equation [40]:

$$G_{ic} = \frac{r_f C_{33s}}{2}\left[\frac{F_c}{\pi r^2} + \frac{(\alpha_f - \alpha_m)\Delta T}{2C_{33s}}\right]^2. \tag{5}$$

The force at debonding initiation point (F_c) is the key value to compute $G_{ic} \cdot C_{33s}$ can be expressed as:

$$C_{33s} = \frac{1}{2}\left(\frac{1}{E_f} + \frac{V_f}{V_m E_m}\right). \tag{6}$$

V_f and V_m are the volume fractions of fiber and matrix, respectively, and E_m is the tensile modulus of matrix. The calculated results for G_{ic} with different concentrations of r-GNF are shown in Figure 11.

TABLE 1 Different Mechanical and Physical Properties of UHMWPE Fiber, Pure Epoxy, and Nano-epoxy Matrix

Property	UHMWPE fiber	Pure epoxy	Nanocomp. 0.1 wt%	Nanocomp. 0.2 wt%	Nanocomp. 0.3 wt%	Nanocomp. 0.5 wt%	Nanocomp. 0.8 wt%
Radius r_f, r_m, mm	0.275	0.5	0.5	0.5	0.5	0.5	0.5
Tensile modulus E_f, E_m GPa	101	1.7	1.7	1.7	1.7	1.7	1.7
Axial shear modulus G_f, G_m GPa	–	0.66	0.66	0.66	0.66	0.66	0.66
CTE below Tg α_m 10–6/°C	210	63.2	60.1	57.4	55.8	54.7	52.9

Note: CTE: coefficient of thermal expansion (CTE); values of CTE of different matrix systems were collected from TMA test [38]. For fiber, the values are collected from the manufacturer. In our previous experiment, very little variation of E_m and G_m values among different matrix systems was observed.

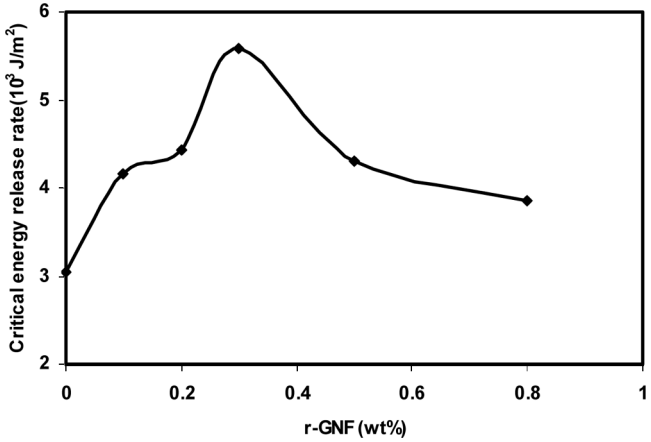

FIGURE 11 Critical energy-release rate *vs*. r-GNF loading.

At 0.3 wt% of r-GNF, the specimen required the highest amount of critical energy for debonding, and its value is increased by $\sim 83\%$ (from 3.05 to $5.59 \times 10^3\,\mathrm{J/m^2}$) over pure epoxy, whereas G_{ic} has lower values for 0.5, 0.8 wt% r-GNF.

From these calculations, the ultimate interfacial shear strength, IFSS, and critical energy-release rate have the highest values in specimens with 0.3 wt% r-GNF, as observed in experimental results, which says that the strongest adhesional bond between matrix and UHMWPE fiber exists with this optimal r-GNF concentration (0.3 wt%) compared with the others.

4. CONCLUSIONS

The adhesion properties between the UHMWPE fibers and the nano-epoxy matrix have been studied through fiber bundle pullout tests. The results showed that the r-GNFs are effective in improving the adhesion between the UHMWPE fibers and the epoxy matrix. The load–displacement curves show four stages—the first corresponds to the elastic elongation of the freelength section of the specimen, the second corresponds to the debonding of the UHMWPE fibers from the matrix in the free length portion, and the third and fourth are mainly related to the debonding and pulling out of the UHMWPE fiber bundle from the matrix, respectively, at the embedded part. In the third stage, there is a change of linearity of load–displacement curves, and a critical point is found where the major fiber/matrix debonding

starts. The specimen containing 0.3 wt% r-GNF loading shows the most effective improvement in interfacial adhesion properties between UHMWPE fiber and matrix. Both experimental and theoretical results agree with each other, and to achieve strong interfacial adhesion between UHMWPE fiber and matrix, optimal concentration of r-GNFs can be recommended.

ACKNOWLEDGMENTS

The authors gratefully acknowledge support from NASA through Grant NNM04AA62G and from the State of North Dakota through NASA EPSCoR and NSF EPSCoR. W. H. Zhong also gratefully acknowledges Charles M. Lukehart and Jiang Li (Vanderbilt University) for providing the derivatized graphitic carbon nanofibers.

REFERENCES

[1] Jang, B. Z., *Advanced Polymer Composites: Principles and Applications* (ASM International, Materials Park, OH, 1994), p. 34.
[2] Ujvari, T., Toth, A., Bertoti, I., Nagy, P. M., and Juhasz, A., *Solid State Ionics* **141–142**, 225–229 (2001).
[3] Torrisi, L., Gammino, S., Mezzasalma, A. M., Visco, A. M., Badziak, J., Parys, P., Wolowski, J., Woryna, E., Laska, L., Pfeifer, M., Rohlena, K., and Boody, F. P., *Applied Surface Science* **227**, 1149–1154 (2004).
[4] Kostov, K. G., Ueda, M., Tan, I. H., Leite, N. F., Beleto, A. F., and Gomes, G. F., *Surface and Coatings Technology* **186**, 287–290 (2004).
[5] Chen, J. S., Lau, S. P., Sun, Z., Tay, B. K., Yu, G. Q., Zhu, Y., Zhu, D. Z., and Xu, H. J., *Surface and Coatings Technology* **138**, 33–38 (2001).
[6] Cohen, Y. D., Rein, M., and Vaykhansky, L., *Composite Science and Technology* **57**, 1149–1154 (1997).
[7] Wang, J. K. and Smith, Jr., J., *Polymer* **40**, 7261–7274 (1999).
[8] Dilsiz, N., Ebert, E., Weisweiler, W., and Akovali, G., *Journal of Colloid and Interface Science* **170**(1), 241–248 (1995)
[9] Drzal, L. and Madhukar, M., *Journal of Material Science* **28**, 569–610 (1993).
[10] Sandler, J., Shafter, T. P., Bauhofer, W., Schulte, K., and Windle, A. H., *Polymer* **40**(21), 5967–5971 (1999).
[11] Yue, Z. R., Jiang, W., Wang, L., Toghiani, H., Gardner, S. D., and Pittman, C. U., *Carbon* **37**, 1607–1618 (1999).
[12] Pittman, C. U., He, G. R., Wu, B., and Gardener, S. D., *Carbon* **35**, 333–340 (1997).
[13] Wong, E. W., Sheehan, P. E., and Lieber, C. M., *Science* **227**, 1971–1975 (1997).
[14] Chen, X. H., Wang, J. X., Yang, H. S., Wu, G. T., Zhang, X. B., and Li, W. Z., *Diamond and Related Materials* **10**, 2057–2062 (2001).
[15] Li, J., Vergne, M. J., Mowlesm, E. D., Zhong, W. H., Hercules, D. M., and Lukehart, C. M., *Carbon* **43**, 2883–2893 (2005).
[16] Vogelson, C. T., Koide, Y., Alemany, L. B., and Barron, A. R., *Chem. Mater.* **12**, 795–804 (2002).
[17] Choi, Y. K., Sugimoto, K., Song, S., Gotoh, Y., Ohkoshi, Y., and Endo, M., *Carbon* **43**, 2199–2208 (2005).

[18] Zilg, C., Dietsche, F., Hoffmann, B., Dietrich, C., and Mülhaupt, R., *Macromol. Symp.* **169**, 65–77 (2001).
[19] Lan, T., Cho, J., and Liang, Y., Maul, P., Applications of nanomer in nanocomposites from concept to reality, Nanocomposites 2001, Chicago, June 25–27, 2001.
[20] Gilbert, E. N., Hayes, B. S., and Seferis, J. C., Nanoparticle modification of epoxy based film adhesives, Proc. SAMPE 2002, Covina, CA, p. 41.
[21] Spindler-Ranta, S. and Bakis, C. E., Carbon nanotube reinforcement of a filament winding resin, Proc. SAMPE 2002, Covina, CA, p. 1775.
[22] Chen, C. and Curliss, D., *SAMPE J.* **37**(5), 11–18 (2001).
[23] Rice, B. P., Chen, C., Cloos, L., and Curliss, D., *SAMPE J.* **37**(5), 7–9 (2001).
[24] Becker, O., Barely, R., and Simon, G., *Polymer* **43**, 4365–4373 (2002).
[25] Becker, O., Cheng, Y. B., Varley, R. J., and Simon, G. P., *Macromolecules* **36**(5), 1616–1625 (2003).
[26] Zhong, W. H., Li, J., Xu, L. R., and Lukehart, C. M., *Polymer Composites* **26**(2), 128–135 (2005).
[27] Wingert, M. T., Improvement of interfacial adhesion between UHMWPE fiber and epoxy matrix using graphitic carbon nanofibers, Masters thesis, North Dakota State University, Fargo, ND (2004).
[28] Neema, S., Zhamu, A., and Zhong, W. H., *Journal of Colloid and Interface Science*, **299**, 332–341 (2006).
[29] Jana, S., Zhamu, A., Gun, Y. X., Zhong, W. H., and Stone, J.J., *Materials and Manufacturing Processes*, in press.
[30] Chua, P. S. and Piggott, M. R., *Composite Science and Technology* **22**, 33–42 (1985).
[31] Piggott, M. R. and Chua, P. S., *Ind. Eng. Chem. Prod. Res. Devel.* **26**, 672–701 (1986).
[32] Piggott, M. R., *Composite Science and Technology* **30**, 295–306 (1987).
[33] Penn, L. S. and Lee, S. M., *J. Compos. Technol. and Res.* **11**, 23–30 (1989).
[34] Valette, L., Rouby, D., and Tallaron, C., *Composite Science and Technology* **62**, 513–518 (2002).
[35] Domnanovich, A., Peterlik, H., and Kromp, K., *Composite Science and Technology* **56**, 1017–1029 (1996).
[36] Desarmot, G. and Favre, J. P., *Composite Science and Technology* **42**, 151–187 (1991).
[37] Chua, P. S. and Piggott, M. R., *Composite Science and Technology* **22**, 107–119 (1985).
[38] Zhamu, A., Hou, Y. P., Zhong, W. H., Stone, J. J., Li, J., and Lukehart, C. M., *Polymer Composites*, in press, 2006.
[39] Gorbatkina, A., *Adhesion Strength of Fiber-Polymer Systems* (Ellis Horwood, New York, 1992).
[40] Pisanov, E., Zhandarov, S., Mader, E., Ahmad, I., and Young, R. J., *Composite: Part A* **32**, 431–446 (2001).
[41] Zhandarov, S., Pisanov, E., and Lauke, B., *Composite Interface*, **5**, 387–404 (1998).